Cell Biol Toxicol (2025) 41:84
https://doi.org/10.1007/s10565-025-10028-4

RESEARCH

U2AF65 mediated circPVT1 promotes NSCLC cell proliferation and inhibits ferroptosis through the miR-338-3p/GPX4 axis

Lujuan He · Zezhi Zhou · Jufen Wang · Jiehan Jiang · Shenggang Liu

Received: 4 November 2024 / Accepted: 13 April 2025

Abstract

Background Dysregulation of circRNA expression is associated with increased metastasis and an adverse prognosis in non-small cell lung cancer (NSCLC). Herein, this study assessed the role and regulatory mechanism of circPVT1 in NSCLC development.

Methods CircPVT1 expression was determined using qPCR. Functional assays, including cell proliferation, colony formation, and ferroptosis-related measurements (ROS, MDA, SOD, GSH and Fe^{2+} levels), were conducted following circPVT1 knockdown. The interactions between RNA and protein were determined through RIP, dual-luciferase reporter and fluorescence in situ hybridization. Actinomycin D assay was employed to test circPVT1 stability. Additionally, tumor progression in vivo was evaluated in xenograft models with U2AF65 knockdown.

Results CircPVT1 was significantly elevated in NSCLC samples, correlating with worse clinical outcomes. Its knockdown resulted in diminished cell proliferation and increased ferroptosis. Mechanically, circPVT1 sponges miR-338-3p, facilitating GPX4 expression, which enhanced cell proliferation. U2AF65 bound to and stabilized circPVT1, promoting cell proliferation. In animal models, U2AF65 knockdown suppressed tumor progression by regulating the circPVT1/miR-338-3p/GPX4 signaling pathway.

Conclusions U2AF65 stabilizes circPVT1 to promote NSCLC advancement through miR-338-3p suppression and GPX4 upregulation. Thus, circPVT1 and U2AF65 may be potential therapeutic targets in NSCLC.

Keywords NSCLC · CircPVT1 · U2AF65 · MiR-338-3p · GPX4 · Ferroptosis

Introduction

Non-small cell lung cancer (NSCLC) is associated with poor prognosis due to increased risk of metastases by the time of diagnosis (Padinharayil and George 2024; Khasraw et al. 2024). Current NSCLC treatment strategies blend personalized targeted and immunotherapies with traditional methods (Favorito et al. 2024; Zhao et al. 2024), however, facing challenges like treatment resistance (Livanou et al. 2024), variable immunotherapy efficacy (Huang et al. 2024), and the critical

Lujuan He and Zezhi Zhou are the co-first authors.

Supplementary Information The online version contains supplementary material available at https://doi.org/10.1007/s10565-025-10028-4.

L. He · Z. Zhou · J. Wang · J. Jiang · S. Liu (✉)
Department of Respiratory and Critical Care Medicine, The Affiliated Changsha Central Hospital, Hengyang Medical School, University of South China, Changsha City 4100007, Hunan Province, P.R. China
e-mail: liushenggang0116@163.com

Published online: 14 May 2025

need for accurate biomarker identification (Hummelink et al. 2022). Ferroptosis, a regulated cell demise (Dixon et al. 2012), can inhibit NSCLC growth when activated, underscoring its significance in diagnosis (Xing et al. 2023). Recent research has highlighted the potential of targeting ferroptosis to overcome resistance to conventional therapies (Ni et al. 2021; Wang et al. 2023), making it a promising avenue for therapeutic intervention in NSCLC. Therefore, investigating ferroptosis mechanisms in NSCLC is crucial for identifying novel biomarkers and advancing therapeutic innovations.

CircRNAs are considered potential biomarkers in human diseases and cancer (Verduci et al. 2021). CircPVT1, a circRNA associated with oncogenesis, has been documented to exhibit critical oncogenic functions in multiple cancer types (Adhikary et al. 2019) and presents a potential prognostic indicator (Zhou et al. 2021). Researches have highlighted its involvement in NSCLC therapy resistance and radiosensitivity (Huang et al. 2021; Wang et al. 2021), yet its precise functional mechanisms in NSCLC remains unclear. Given the association of circPVT1 with the ferroptosis pathway (Yao et al. 2021), its role in NSCLC may be attributed to its capacity to modulate ferroptosis, a hypothesis that warrants further investigation.

In exploring the mechanisms of circRNA, its role as a molecular sponge is frequently investigated and highlighted (Hansen et al. 2013). Our early study explored the sponge-like function of circPVT1, which can further sponge miR-338-3p. Furthermore, glutathione peroxidase 4 (GPX4) was recognized as a potential downstream effector of this microRNA. Since GPX4 is a critical molecule in the ferroptosis pathway (Seibt et al. 2019), miR-338-3p is likely involved in regulating ferroptosis in NSCLC. MiR-338-3p has been demonstrated to inhibit NSCLC proliferation and metastasis (Tian et al. 2022). However, its precise mechanisms within NSCLC and its interplay with ferroptosis necessitates further research.

CircRNAs are regulated by RNA-binding proteins (RBPs), crucial for RNA transcription, splicing, modification, and translation (Okholm et al. 2020). Here, we discovered that U2AF65 could serve as a potential RBP of circPVT1. U2AF65 due to its upregulation in NSCLC cells and high risk of malignant progression (Li et al. 2019), yet its mechanism and interaction with circPVT1 are still to be clarified.

Therefore, this study focused on investigating circPVT1's involvement in NSCLC advancement, aiming to elucidate its mechanism involving U2AF65, miR-338-3p, and GPX4 mRNA, and further explored this interaction with the ferroptosis pathway. Unraveling these mechanisms might identify potential biomarkers for targeting ferroptosis in NSCLC treatment, offering prospects for the development of ferroptosis-based therapeutic strategies.

Methods

Clinical sample collections

Tumor and adjacent non-malignant tissues were obtained from 30 NSCLC individuals undergoing surgical excision. Tumor samples were taken from the primary site, while non-cancerous tissues were collected from regions adjacent to the tumor. All samples were collected immediately post-surgery and placed in sterile containers. They were promptly transported on ice to the laboratory and preserved at − 80 °C. Signed patients' consent were obtained, and ethic approval was obtained from the Ethics Committee of The Affiliated Changsha Central Hospital, Hengyang Medical School, University of South China (No. 2022-S0181).

Cell culture

A549, HCC827, NCI-H1650, H2170, and NCI-H446 cell lines were acquired through the American Type Culture Collection (#CCL- 185, #CRL- 2868, #CRL-5883, #CRL- 5928, #HTB- 171, respectively, Virginia, USA), while the 16HBE cell line was obtained from Sigma-Aldrich (#SCC150, MO, USA). All cultures were maintained in DMEM (#11965092, Gibco, NY, USA), enriched with 10% FBS (#16000044, Gibco) and 1% penicillin–streptomycin solution (#15140122, Thermo Fisher, MA, USA), followed by incubation (37 °C, 5% CO_2, changing medium every 2–3 d). Cells were passaged at 70–80% confluency, washed with PBS, trypsinized for 5 min at 37 °C, neutralized with fresh medium, followed by

centrifugation (1000 rpm, 5 min), and reseeded (1×10^5 cells/cm^2) in new T25 flasks.

Cell transfection

Vectors for knockdown (sh-NC, sh-circPVT1, sh-GPX4, sh-U2AF65) and overexpression (pc-NC, pc-circPVT1, pc-U2AF65) RNAs were constructed using standard molecular cloning techniques. Target sequences for shRNAs were inserted into the pLKO.1 vector (#8453, Addgene, MA, USA), while cDNA for overexpression constructs was inserted into the pcDNA3.1 vector (#V79020, Invitrogen, CA, USA).

Then, cells (2×10^5) were cultured to 70–80% confluency before transfection. For transfection, plasmid DNA and Lipofectamine® 2000 Reagent (#11668019, Thermo Fisher) were mixed with Opti-MEM® (#31985070, Gibco) and left at room temperature for 20 min to form complexes. These complexes were then introduced into the cells and left for incubation for 6 h before the old medium was replaced. After 48 h, cells were harvested. The target sequences are shown in Supplementary Table S1.

Quantitative PCR (qPCR)

Cellular RNA was removed using TRIzol (#15596026, Invitrogen) and 1 μg of RNA was reverse transcribed for circPVT1, GPX4 and U2AF65 (PrimeScript™ RT Kit, #RR037 A, Takara, Shiga, Japan). MiR-338-3p was converted to cDNA using the Mir-X™ miRNA First-Strand Synthesis Kit (#638315, Takara). SYBR® Premix Ex Taq™ II Kit (#RR820 A, Takara) on an ABI 7500 system was used for qPCR (conditions: intial denaturation, 95 °C, 30 s; 40 cycles at 95 °C, 5 s and 60 °C, 34 s). Expression levels quatification was conducted ($2^{-\Delta\Delta CT}$) and normalized circPVT1, GPX4, and U2AF65 to GAPDH, and miR-338-3p to U6. Primers were listed in Table 1.

CCK- 8 assay

Cells (5×10^3/well) were placed in a 96-well plate overnight and treated with CCK- 8 reagent (10 μL, #CK04, Dojindo, Kumamoto, Japan) every 24 h for 4 h at 37 °C for 3 days and assessed at 450 nm wavelength.

Clonogenic assay

We placed cells (500/well) in 4-well dishes and treated them at conditions above for 14 d and replaced the medium after each following day. Colonies were fixed (4% paraformaldehyde), stained (0.5% crystal violet), rinsed with PBS, and analyzed microscopically if containing at least 30 cells.

DCFH-DA staining for detection of ROS

Cells (1×10^5/well, 6-well plates) were treated using DCFH-DA (10 μM, #D6883, Sigma-Aldrich) in medium without serum and light at 37 °C for 30 min and washed thrice using PBS. ROS levels were detected using a fluorescence microscope (485 nm excitation, 535 nm emission).

MDA, SOD, GSH, and Fe^{2+} assessment

Cells were homogenized and the supernatant was retrieved after centrifugation (10,000 ×g, 10 min). For malondialdehyde (MDA) detection, the MDA Assay Kit (#MAK085, Sigma-Aldrich) was used, and absorbance was recorded at 532 nm. Superoxide dismutase (SOD) activity was examined with the SOD Assay Kit (#19160, Sigma-Aldrich), with absorbance read at 450 nm. Glutathione (GSH) levels were determined using the GSH Assay Kit (#CS0260, Sigma-Aldrich), with absorbance measured at 412 nm. Fe^{2+} levels were measured using the Iron Assay Kit (#MAK025, Sigma-Aldrich), with absorbance read at 593 nm. Measured concentrations were compared to standard curves.

Western blot

The cells were lysed (RIPA buffer, #89900, Thermo Fisher; protease inhibitors, #P8340, Sigma-Aldrich), and quantified (BCA kit, #23225, Thermo Fisher). Protein (20 μg) were loaded onto SDS-PAGE (Bio-Rad, CA, USA), then transferred to PVDF membranes (#IPVH00010, Millipore, MA, USA), and blocked in TBST with 5% non-fat milk, followed by overnight incubation (at 4 °C) with primary antibodies against ACSL4 (#ab155282, Abcam, Cambridge,

Table 1 Primer sequences used for qPCR

Name	Forward (5'– 3')	Reverse (5'– 3')
circPVT1	CTATGGAATGTAAGACCCCGA	GCTCAGAAAATACTTGAACGA
GPX4	ACAAGAACGGCTGCGTGGTGAA	GCCACACACTTGTGGAGCTAGA
U2AF65	CGGCAGCTCAACGAGAATAAA	GGGAACGAATCAGTCCACCG
miR-338-3p	TGCGGTCCAGCATCAGTGATTTTGTT	CCAGTGCAGGGTCCGAGGT
U6	CTCGCTTCGGCAGCACA	AACGCTTCACGAATTTGCGT
GAPDH	GGAGCGAGATCCCTCCAAAAT	GGCTGTTGTCATACTTCTCATGG

UK), SLC7 A11 (#12691, Cell Signaling Technology, MA, USA), Prominin 2 (PROM2, #HPA042440, Sigma-Aldrich), GPX4 (#ab125066, Abcam), U2AF65 (#ab37530, Abcam) and GAPDH (#2118, Cell Signaling Technology). Next, they were treated using HRP-linked secondary antibodies (#7074 and #7076, Cell Signaling Technology) for 1 h at ambient temperature. Bands were detected using ECL reagent (#32106, Thermo Fisher) and visualized (Bio-Rad chemiluminescent imaging system). Protein levels were normalized to a GAPDH protein for analysis.

Transmission electron microscopy (TEM)

Cells were immobilized in glutaraldehyde (#G5882, Sigma-Aldrich) at 4 °C for 2 h, then fixed with 1% osmium tetroxide (#75632, Sigma-Aldrich) for 1 h, sequentially dehydrated with increasing ethanol concentrations, and transferred to propylene oxide (#296000, Sigma-Aldrich), before being embedded in Epon resin (#14120, Electron Microscopy Sciences, PA, USA). Sections of 70 nm thickness were prepared, stained with a mixture of uranyl acetate and lead citrate (#73943, Sigma-Aldrich) and assessed (JEOL transmission electron microscopy, Tokyo, Japan) to visualize mitochondrial structures.

Dual-luciferase reporter assay

The Starbase software (https://rnasysu.com/encori/) was used to predict potential binding sites of circPVT1 or GPX4 with miR-338-3p. Cells (1×10^5 cells/well) were plated into 24-well plates and subsequently co-transfected with 50 ng of luciferase reporter constructs circPVT1-WT, circPVT1-MUT, GPX4-WT, or GPX4-MUT, custom cloned into the pGL3-Basic vector (Promega, WI, USA) and 50 nM miR-338-3p mimic (HY-R00698, MCE, NJ, USA). Renilla luciferase plasmid pRL-TK (#E2241, Promega) served as an internal control. Transfection was performed utilizing Lipofectamine® 2000 (#11668019, Thermo Fisher) in Opti-MEM® (#31985070, Gibco). After 48 h, cells were collected, and luciferase activity was quantified (#E1910, Promega), and normalized to Renilla.

Fluorescence in situ hybridization (FISH)

Cells were placed on glass coverslips until adherence, fixed (4% paraformaldehyde) for 15 min, permeabilized in 0.1% Triton X- 100 (#X100, Sigma-Aldrich) for 10 min, and incubated at 37 °C overnight with fluorescent probes for circPVT1 and miR-338-3p (Qiagen, Venlo, Netherlands) in hybridization buffer. Following hybridization, the slides were washed, nuclei stained using DAPI (#D9542, Sigma-Aldrich), placed on ProLong™ Gold Antifade Mountant (#P36930, Thermo Fisher) and assessed using fluorescence microscopy (Zeiss, Oberkochen, Germany) and ImageJ.

RNA immunoprecipitation (RIP)

After lysis in RIPA with RNase inhibitor (#R9153, Sigma-Aldrich), lysates were incubated with anti-Ago2 antibody (#ab32381, Abcam) bound to Dynabeads™ Protein A (#10002D, Thermo Fisher). After incubation overnight at 4 °C, beads were rinsed in RIPA, we separated bound RNA with TRIzol™ (#15596026, Thermo Fisher). Subsequently, cDNA was synthesized with PrimeScript™ RT Reagent Kit (#RR037 A, Takara). qPCR analysis was conducted utilizing SYBR® Premix Ex Taq™ II (#RR820 A, Takara) for quantifying circPVT1, miR-338-3p, and GPX4 levels.

Actinomycin D assay

Cells were grown to 70–80% confluence in 6-well plates, treated with 5 µg/mL actinomycin D (#A1410, Sigma-Aldrich) to halt transcription, and collected at

0, 2, 4, 6, 8, and 10 h. RNA was extracted with TRIzol™ Reagent (#15596026, Thermo Fisher), reverse transcribed using the PrimeScript RT Kit (#RR037 A, Takara), and circPVT1 expression was quantified by qPCR with SYBR Premix Ex Taq II (#RR820 A, Takara), normalized to GAPDH.

Xenograft tumor model

H2170 cells (5×10^6) were mixed with PBS (Gibco) and Matrigel (Corning) at a 1:1 ratio and implanted into anesthetized male BALB/c nude mice's flanks (6–8 weeks, $n = 6$/group). The tumors were monitored biweekly with calipers, and volume determined as $0.5 \times \text{Length} \times \text{Width}^2$. They were sacrificed on 28 th day to retrieve the tumors. Approval was obtained from The Affiliated Changsha Central Hospital Ethics Committee (No. 2022-S0181).

Hematoxylin and eosin (H&E) staining

After kept in 10% formalin overnight, the tissues were embedded in paraffin, cut into 5 μm sections, deparaffinized in xylene, rehydrated with graded ethanol, stained with hematoxylin (#HHS16, Sigma-Aldrich) for 5 min, rinsed, counterstained with eosin (#HT110216, Sigma-Aldrich) for 1 min, dehydrated, cleared, mounted using Permount (#SP15 -100, Fisher Chemical), and assessed using light microscopy.

Immunohistochemistry (IHC)

Tumor tissue sections were cleared with xylene and rehydrated through graded ethanol solutions. Antigen epitopes were unmasked by heating the sections in a citrate buffer. Endogenous peroxidase activity was blocked in 3% hydrogen peroxide, followed by incubation with 10% normal goat serum, and overnight at 4 °C with antibodies targeting Ki- 67 (#ab16667, Abcam), U2AF65 (#ab37530, Abcam), GPX4 (#ab125066, Abcam), and ACSL4 (#ab155282, Abcam). After washing, an HRP-conjugated secondary antibody (#P0448, Dako) was applied. The immune complexes were visualized using a DAB substrate (#K3468, Dako), and counterstained with hematoxylin (#HHS16, Sigma-Aldrich). Finally, sections were dehydrated, cleared, and mounted for examination under a Zeiss light microscope.

Statistical analysis

Experiments were conducted in triplicate unless stated otherwise. Data were analyzed using GraphPad Prism 9.0 and shown as mean ±SD. Student's t-test (two groups) or one-way ANOVA with Tukey's test (multiple groups) were used to determine difference between groups, correlations were assessed with Pearson's coefficient and $P < 0.05$ was considered for significance.

Results

Upregulation of circPVT1 in NSCLC associates with poor prognosis

To ascertain circPVT1 in NSCLC, we analyzed its expression patterns in NSCLC tissues versus paracancer tissues and observed increased expressions in NSCLC samples compared to paracancer ones (Fig. 1A). Corroborating this, an upregulation of circPVT1 was also observed in NSCLC cells relative to 16HBE cells (Fig. 1B). Additionally, high expression of circPVT1 was correlated with tumor size, TNM stage, and lymph node metastasis (Table 2). Moreover, this high expression was associated with shorter overall survival (Fig. 1C). These results indicate that elevated circPVT1 expression correlates with a poor prognostic outcome.

CircPVT1 enhances NSCLC cell proliferation and suppresses ferroptosis

To elucidate the functional significance of circPVT1 in NSCLC, circPVT1 was selectively downregulated in A549 and A2170 cell lines (Fig. 2A). This intervention notably attenuated cellular proliferation (Fig. 2B-C). Considering the regulatory role of circPVT1 in tumor ferroptosis (Yao et al. 2021), a critical mechanism underlying NSCLC pathogenesis (Gao et al. 2024), we proceeded to evaluate the impact of circPVT1 on ferroptosis. The silence of circPVT1 expression significantly augmented levels of ROS, MDA, and Fe^{2+}, while simultaneously diminishing the concentrations of SOD and GSH (Fig. 2D-H).

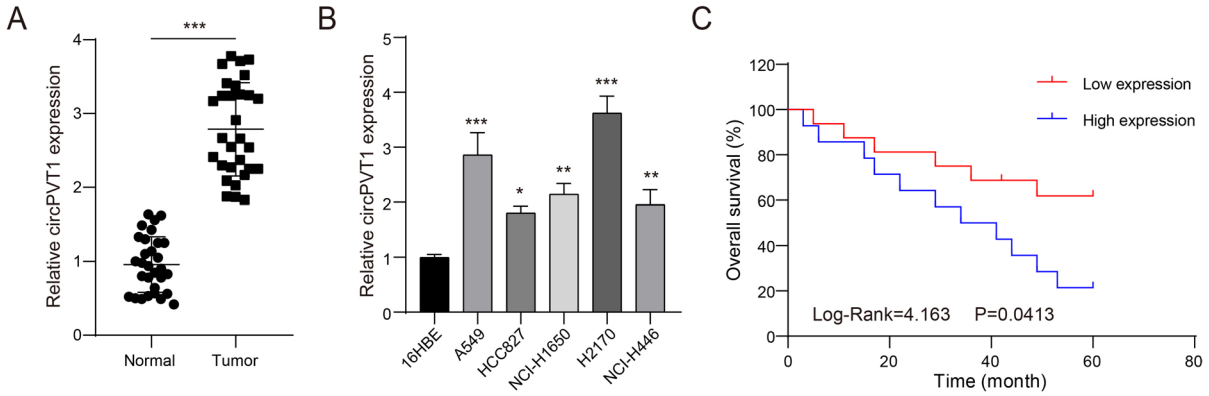

Fig. 1 Upregulation of circPVT1 in NSCLC associates with poor prognosis. **A** qPCR analysis of circPVT1 expression levels in NSCLC tissues and paracancer tissues. **B** qPCR analysis of circPVT1 expression levels in 16HBE cells and NSCLC cells. **C** Kaplan–Meier analysis of overall survival based on circPVT1 expression levels. $*P < 0.05$, $**P < 0.01$, $***P < 0.001$

Moreover, circPVT1 inhibition correlated with increased ACSL4 expression while leading to the downregulation of SLC7 A11 and PROM2 (Fig. 2I), all of which are proteins implicated in the ferroptosis pathway. Furthermore, knockdown of circPVT1 led to the contraction or disappearance of

Table 2 Correlation between circPVT1 expression and clinicopathological characteristics of NSCLC patients ($N = 30$)

Characteristics	Total number	Low expression ($n = 15$)	High expression ($n = 15$)	*P* value
Age				0.4621
< 60	13	8	5	
≥ 60	17	7	10	
Gender				0.1281
Male	19	7	12	
Female	11	8	3	
Smoke				0.7104
Yes	12	5	7	
No	18	10	8	
Drink				0.6999
Yes	20	9	11	
No	10	6	4	
Histology				0.2723
Adenocarcinoma	14	9	5	
Squamous	16	6	10	
Tumor size				0.0253
< 3	13	10	3	
≥ 3	17	5	12	
TNM stage				0.0025
I-II	17	13	4	
III-IV	13	2	11	
Lymph nodes metastasis				0.0078
Yes	12	2	10	
No	18	13	5	

mitochondrial cristae (Fig. 2J). We also observed that overexpression of circPVT1 in HCC827 cells resulted in the opposite effects, including promoted cell proliferation, reduced levels of ROS, MDA, and Fe^{2+}, and an increase in SOD and GSH levels (Supplementary Fig. 1). These findings underscore the critical function of circPVT1 in modulating ferroptosis and NSCLC pathogenesis.

CircPVT1 sponges miR-338-3p

Given the essential role of circRNA as a molecular sponge for targeting miRNA(Kamali et al. 2024), we aimed to identify the target miRNA of circPVT1. Prediction analysis had indicated a potential interaction between circPVT1 and miR-338-3p (Fig. 3A). Also, this microRNA

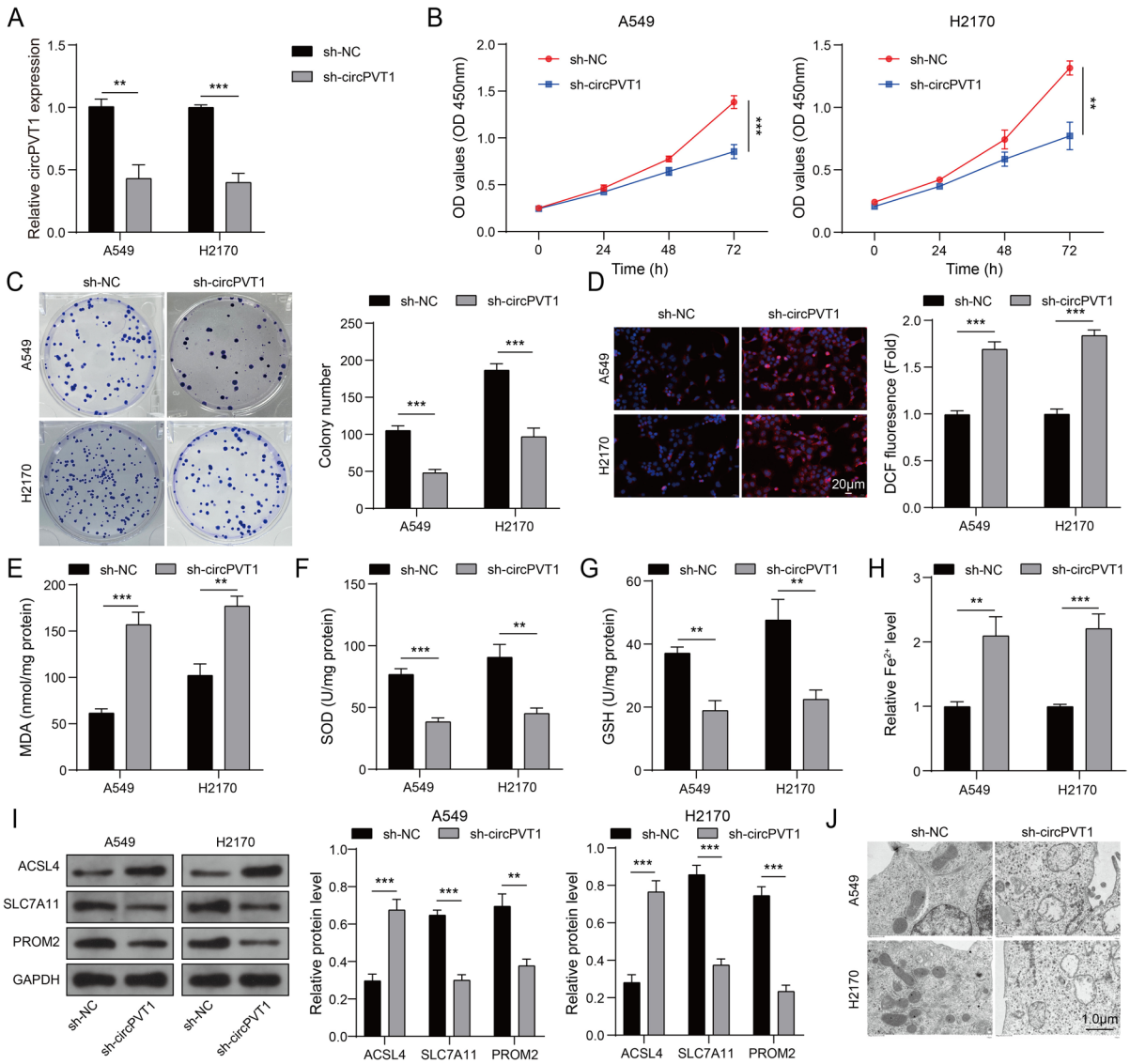

Fig. 2 CircPVT1 enhances NSCLC cell proliferation and suppresses ferroptosis. Knockdown of circPVT1 in A549 and A2170 cells was performed. **A** qPCR analysis of circPVT1 expression. **B** CCK- 8 assay to measure cell proliferation. **C** Colony formation assay to assess cell proliferation. **D** DCFH-DA staining to detect ROS levels. Kit assays to measure (**E**) MDA levels, **F** SOD levels, **G** GSH levels and (**H**) Fe^{2+} levels. **I** Western blot analysis to detect protein expression of ACSL4, SLC7 A11, and PROM2. **J** TEM observation of mitochondrial morphology. $^{**}P < 0.01$, $^{***}P < 0.001$

mimic reduced the luciferase activity of wild-type circPVT1 but not of mutant circPVT1 (Fig. 3B). FISH indicated the cytoplasmic presence of circPVT1 and miR-338-3p (Fig. 3C). Furthermore, the circPVT1 interacts with miR-338-3p within the RNA complex (Fig. 3D). Additionally, circPVT1 knockdown promoted miR-338-3p expression (Fig. 3E). Interestingly, miR-338-3p was downregulated in NSCLC, displaying an inverse correlation with circPVT1 expression (Fig. 3F-H), demonstrating circPVT1 could sponge miR-338-3p to suppress its expression in NSCLC.

Fig. 4 CircPVT1 sponges miR-338-3p to upregulate GPX4 expression. **A** Starbase (https://rnasysu.com/encori/) predicted potential binding sites between miR-338-3p and GPX4. **B** Dual-luciferase reporter assays confirmed the interaction between miR-338-3p and GPX4. **C** RIP assays examined the binding of Ago2 with miR-338-3p and GPX4. **D** qPCR measured miR-338-3p expression after overexpression or knockdown of miR-338-3p. **E** qPCR detected GPX4 mRNA expression. **F** western blot measured GPX4 protein expression. **G** qPCR measured GPX4 mRNA expression in NSCLC tissues and paracancer tissues. **H** western blot detected GPX4 protein expression in NSCLC tissues and paracancer tissues. **I** Western blot detected GPX4 protein expression in 16HBE cells and NSCLC cells. **J-K** Pearson correlation analysis evaluated the correlation between miR-338-3p and GPX4 expression, as well as the correlation between circPVT1 and GPX4 expression. $^{*}P < 0.05$, $^{**}P < 0.01$, $^{***}P < 0.001$

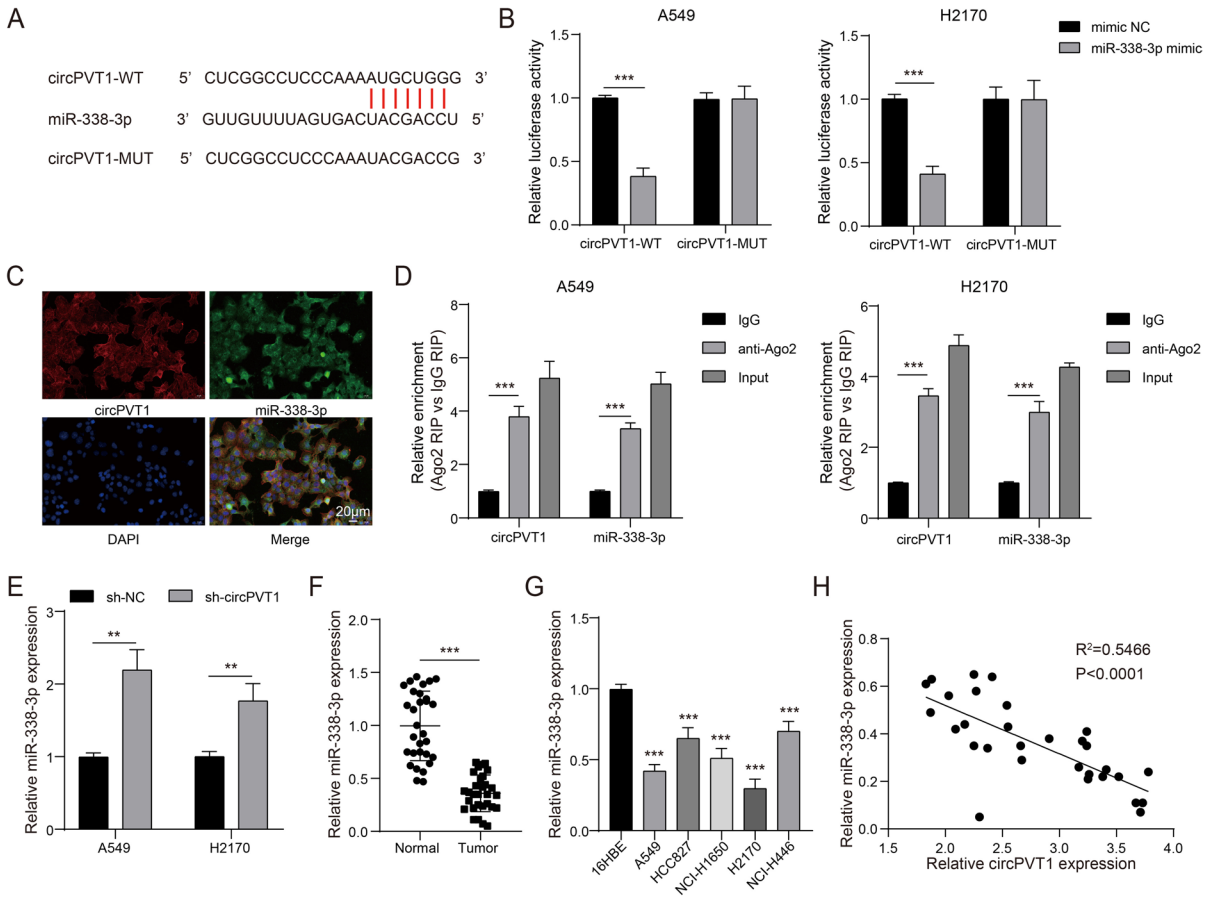

Fig. 3 CircPVT1 sponges miR-338-3p. **A** Starbase (https://rnasysu.com/encori/) predicted potential binding sites between circPVT1 and miR-338-3p. **B** Dual-luciferase reporter assays confirmed the interaction between miR-338-3p and circPVT1. **C** FISH detected the colocalization of circPVT1 and miR-338-3p in H2170 cells. **D** RIP assays examined the binding of circPVT1 and miR-338-3p to Ago2. **E** qPCR assessed miR-338-3p expression after circPVT1 knockdown. **F** qPCR detected miR-338-3p expression in NSCLC tissues and paracancer tissues. **G** qPCR measured miR-338-3p expression in 16HBE cells and NSCLC cells. **H** Pearson correlation analysis evaluated the correlation between circPVT1 and miR-338-3p expression in tissues. $^{**}P < 0.01$, $^{***}P < 0.001$

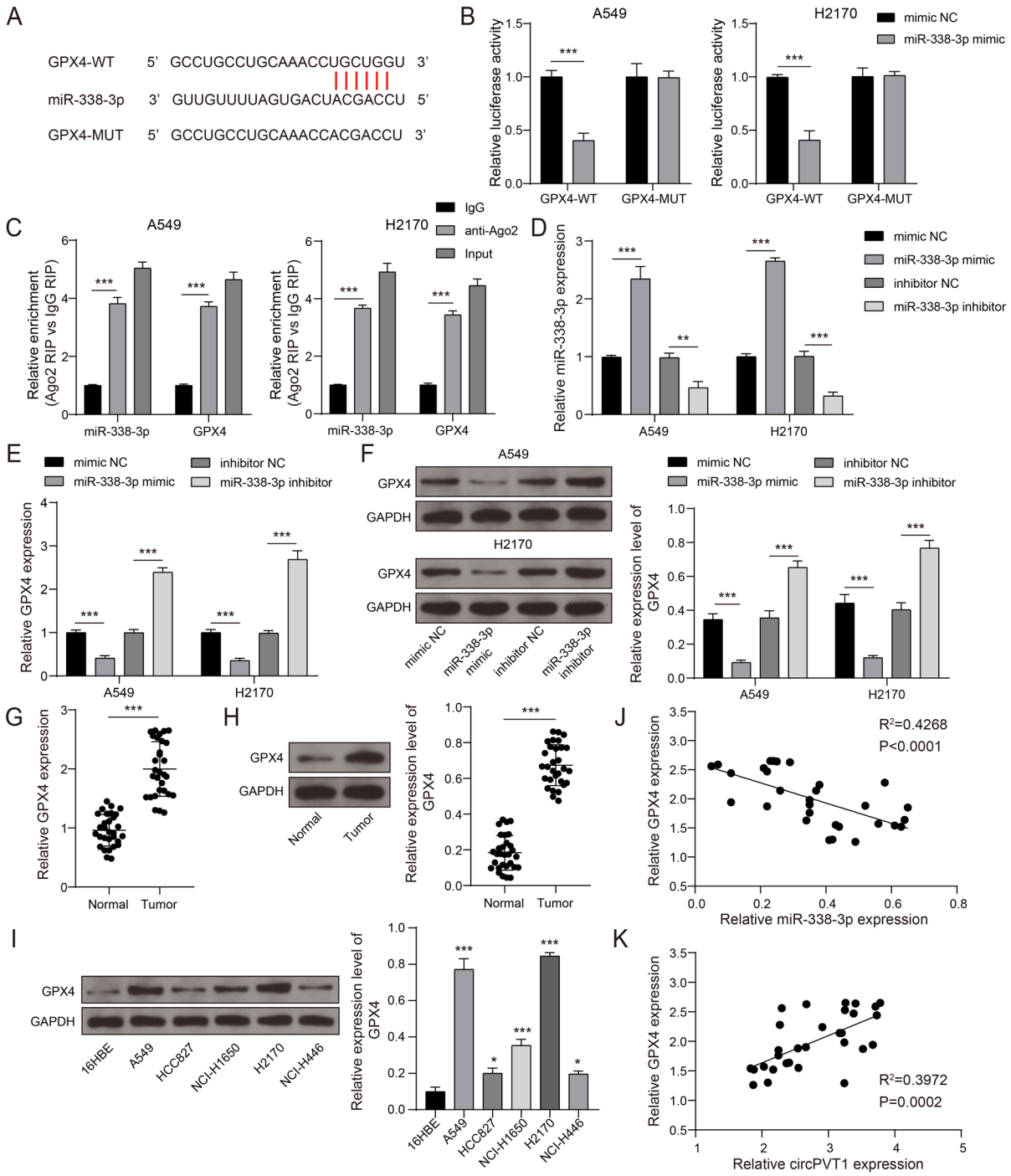

CircPVT1 sponges miR-338-3p to elevate GPX4 expression

Since circPVT1 mediated the progression of ferroptosis in NSCLC, it may influence proteins that related to ferroptosis. Therefore, we explored the potential regulation of GPX4 expression, a critical protein in the ferroptosis pathway (Dos Santos et al. 2023), by miR-338-3p. Prediction analysis revealed a promising interaction between miR-338-3p and GPX4 (Fig. 4A).

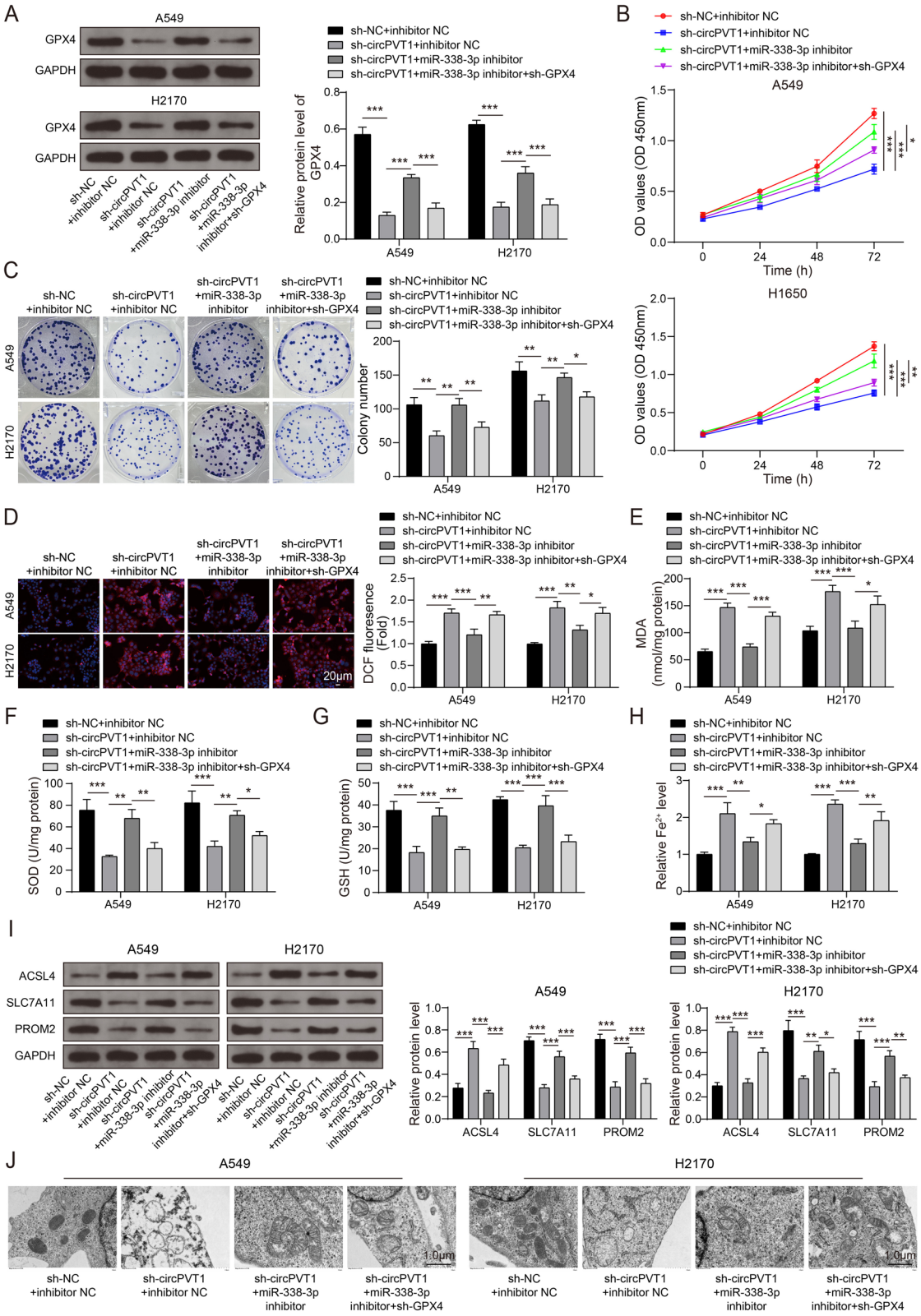
A
A549
GPX4
GAPDH
H2170
sh-NC +inhibitor NC
sh-circPVT1 +inhibitor NC
sh-circPVT1 +miR-338-3p inhibitor
sh-circPVT1 +miR-338-3p inhibitor+sh-GPX4
Relative protein level of GPX4
B
OD values (OD 450nm)
Time (h)
H1650
C
Colony number
D
DCF fluorescence (Fold)
20μm
E
MDA (nmol/mg protein)
F
SOD (U/mg protein)
G
GSH (U/mg protein)
H
Relative Fe2+ level
I
ACSL4
SLC7A11
PROM2
Relative protein level
J
1.0μm

◂**Fig. 5** CircPVT1 promotes NSCLC cell proliferation and inhibits ferroptosis by modulating miR-338-3p/GPX4 axis. In A549 and H2170 cells, circPVT1 was knocked down and/or miR-338-3p was inhibited, followed by GPX4 knockdown: **A** Western blot was used to detect GPX4 protein expression. **B** CCK- 8 assays measured cell proliferation. **C** Colony formation assays assessed cell proliferation. **D** DCFH-DA staining detected ROS levels. **E–H** Kits measured levels of MDA, SOD, GSH, and Fe^{2+}. **I** Western blot detected the expression of ACSL4, SLC7 A11, and PROM2 proteins. **J** TEM observed mitochondrial morphology. $*P < 0.05$, $**P < 0.01$, $***P < 0.001$

Also, the miR-338-3p mimic specifically targets and regulates GPX4 by binding to its wild-type sequence (Fig. 4B). The RNA complex precipitated by Ago2 pull-down showed a notable enrichment of this microRNA and GPX4 (Fig. 4C). The overexpression and knockdown cell model of miR-338-3p was successfully carried out (Fig. 4D). Interestingly, miR-338-3p upregulation also reduced GPX4 levels, while knockdown increased them (Fig. 4E-F). In tumor tissues, GPX4 mRNA (Fig. 4G) and protein levels (Fig. 4H) were upregulated compared to paracancer tissues. GPX4 protein was also higher in NSCLC cells relative to 16HBE cells (Fig. 4I). GPX4 expression and miR-338-3p were shown to be inversely correlated, while circPVT1 and GPX4 levels were positively correlated (Fig. 4J-K). These studies demonstrate that circPVT1 sponges miR-338-3p to upregulate GPX4.

CircPVT1 promotes NSCLC cell growth and inhibits ferroptosis by modulating miR-338-3p/GPX4 axis

We further found that silencing circPVT1 resulted in GPX4 downregulation, which was counteracted by miR-338-3p suppression; inhibiting this RNA elevated GPX4 expression, an outcome negated by GPX4 knockdown (Fig. 5A). Functional studies indicated that silencing circPVT1 diminished cell proliferation, effects that were reversed upon miR-338-3p inhibition. Conversely, this microRNA inhibition enhanced cell growth, outcomes that were negated following GPX4 knockdown (Fig. 5B-C). Additional experiments showed that circPVT1 knockdown increased ROS, MDA, and Fe^{2+} levels, while reducing SOD and GSH concentrations, effects that were counteracted by miR-338-3p inhibition. Inhibition of this microRNA exhibited opposite effects on ROS, MDA, Fe^{2+}, SOD, and GSH compared to circPVT1 silencing, which were nullified by GPX4 knockdown (Fig. 5D-H). Furthermore, circPVT1 suppression led to ACSL4 upregulation with SLC7 A11 and PROM2 downregulation, which were counteracted by miR-338-3p inhibition. Similarly, this microRNA inhibition showed contrasting effects, which were mitigated by GPX4 suppression (Fig. 5I). CircPVT1 knockdown resulted in the contraction or disappearance of mitochondrial cristae, a scenario counteracted by miR-338-3p inhibition. However, this microRNA inhibition produced opposing outcomes, which were abolished by GPX4 knockdown (Fig. 5J). These findings underscore the circPVT1/miR-338-3p/GPX4 axis in driving NSCLC progression and modulating ferroptosis.

U2AF65 binds to circPVT1 and stabilizes it

CircRNAs can be regulated by RBPs, thus the upregulation of circPVT1 may be modulated by its associated RBPs. Prediction analysis identified promising RBPs for circPVT1, including EIF4 A3 and U2AF65 (Fig. 6A). Although both EIF4 A3 and U2AF65 expressions were increased in NSCLC tissues (Fig. 6B), only U2AF65 expression correlated with circPVT1, exhibiting a positive association (Fig. 6C). We also verified that U2AF65 expression was elevated in NSCLC cells (Fig. 6D-E). Molecular experiments revealed that U2AF65 bound to circPVT1 and positively regulated its expression (Fig. 6F-G). Furthermore, overexpression of U2AF65 significantly enhanced the stability of circPVT1 (Fig. 6H). These results suggest that U2AF65 binds to circPVT1, stabilizing and enhancing its expression in NSCLC.

U2AF65 enhances NSCLC cell proliferation and suppresses ferroptosis by stabilizing circPVT1

Experiments showed that U2AF65 overexpression enhanced cell proliferation, which were negated upon circPVT1 silencing (Fig. 7A-B). Additionally, overexpression of U2AF65 reduced ROS, MDA, and Fe^{2+} levels, while increasing SOD and GSH concentrations, outcomes counteracted by circPVT1 knockdown (Fig. 7C-G). Moreover, U2AF65 overexpression

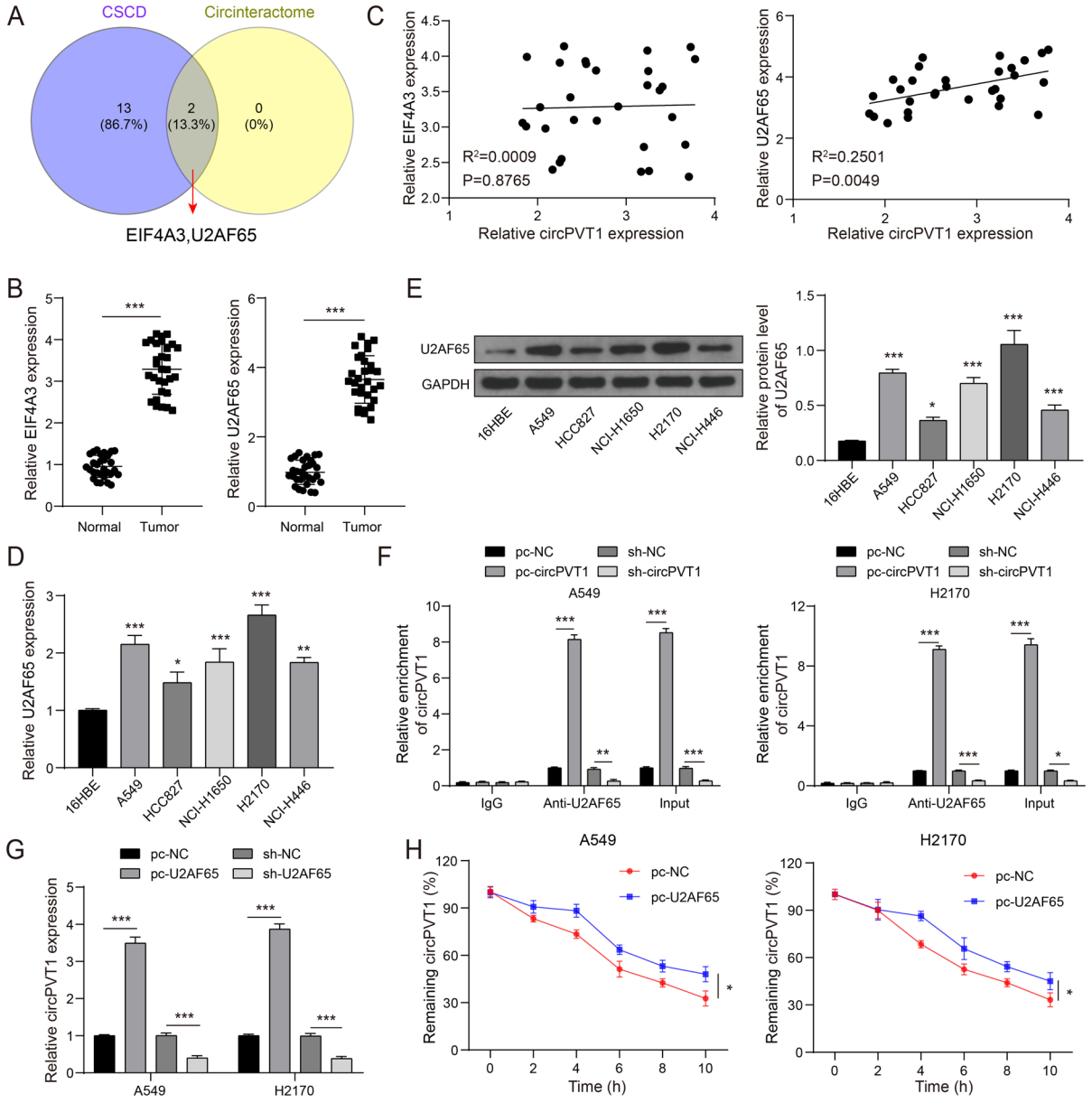

Fig. 6 U2AF65 binds to circPVT1 and stabilizes it. **A** CSCD (http://gb.whu.edu.cn/CSCD/) and CircInteractome (https://circinteractome.nia.nih.gov/circular_rna.html) predicted RBPs interacting with circPVT1. **B** qPCR was used to detect the expression of EIF4 A3 and U2AF65 in NSCLC tissues and paracancer tissues. **C** Pearson correlation analysis evaluated the correlation between EIF4 A3 expression and circPVT1, as well as between U2AF65 expression and circPVT1. **D** qPCR was used to detect the expression of U2AF65 in 16HBE cells and NSCLC cells. **E** Western blot detected U2AF65 protein expression in 16HBE cells and NSCLC cells. **F** RIP assays detected the interaction between circPVT1 and U2AF65. **G** qPCR measured the expression of circPVT1. **H** Actinomycin D assay determined the half-life of circPVT1. $^{*}P < 0.05$, $^{**}P < 0.01$, $^{***}P < 0.001$

decreased ACSL4 but increased SLC7 A11 and PROM2 expression, effects were mitigated when simultaneously silencing circPVT1 (Fig. 7H). Knockdown of circPVT1 also reversed the protective effect of U2AF65 on the shrinkage or disappearance of mitochondrial cristae (Fig. 7I). Overall, these results highlight that U2AF65

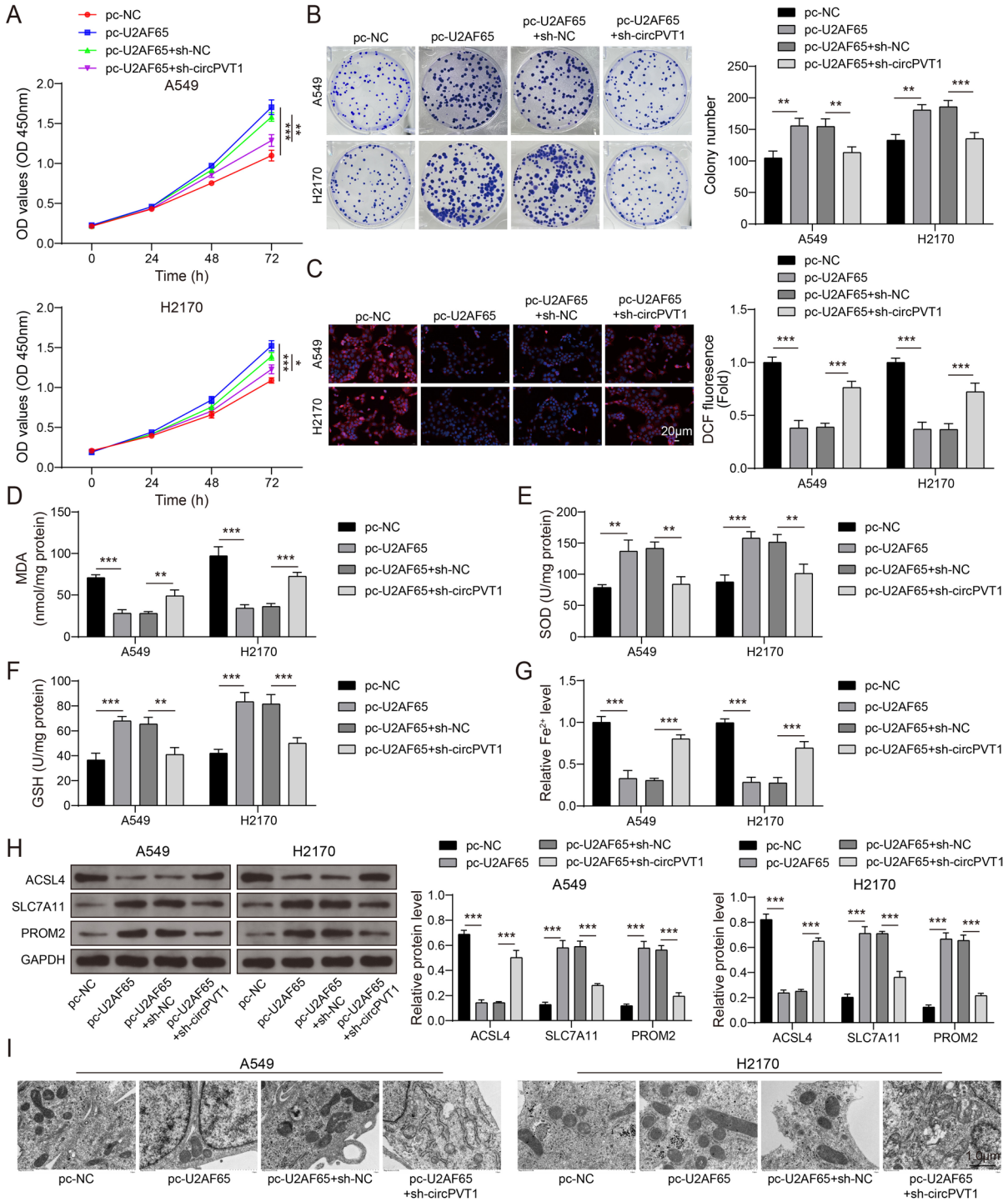

Fig. 7 U2AF65 enhances NSCLC cell proliferation and suppresses ferroptosis by stabilizing circPVT1. In A549 and H2170 cells, U2AF65 was overexpressed or circPVT1 was simultaneously knocked down: **A** CCK- 8 assays were used to measure cell proliferation. **B** Colony formation assays assessed cell proliferation. **C** DCFH-DA staining detected ROS levels. **D-G** Kits were used to measure the levels of MDA, SOD, GSH, and Fe^{2+}. **H** Western blot detected the expression of ACSL4, SLC7 A11, and PROM2 proteins. **I** TEM was used to observe mitochondrial morphology. $^{*}P < 0.05$, $^{**}P < 0.01$, $^{***}P < 0.001$

promotes NSCLC cell proliferation and inhibits ferroptosis by stabilizing circPVT1.

U2AF65 promotes NSCLC tumorigenesis via the circPVT1/miR-338-3p/GPX4 axis

In vivo studies revealed that knockdown of U2AF65 significantly impeded tumorigenesis, as demonstrated by reduced size and weight of tumor nodules (Fig. 8A-C). Moreover, silencing U2AF65 decreased Ki- 67, U2AF65, and GPX4 expressions while promoting the ACSL4 expression (Fig. 8D). Additionally, the suppression of U2AF65 resulted in decreased of circPVT1 expression while enhancing miR-338-3p expression (Fig. 8E). These in vivo findings corroborate that U2AF65 facilitates NSCLC tumorigenesis through the circPVT1/miR-338-3p/GPX4 axis.

Discussion

Recent progress in ferroptosis research within NSCLC highlights its crucial role in tumor biology, focusing on iron metabolism (Wang et al. 2024), lipid peroxidation (Chen et al. 2024), and the regulatory function of proteins like GPX4 (Li et al. 2024). Insights into the relationship between ferroptosis and therapy resistance have opened new therapeutic avenues (Han et al. 2024), emphasizing the potential of ferroptosis inducers in NSCLC treatment strategies. Researches on circRNA's role in ferroptosis regulation reveal its capacity to modulate iron metabolism and lipid peroxidation pathways by sponging miRNAs that target ferroptosis-related genes like GPX4 (Arabpour et al. 2024; Li et al. 2024). This highlights circRNA's potential in influencing ferroptosis and opens new avenues for cancer therapy, particularly in NSCLC.

This research has elucidated that upregulated circPVT1 in NSCLC is linked to poor clinical outcomes, facilitating cell growth while inhibiting ferroptosis. Previous investigations have underscored circPVT1's oncogenic potential in NSCLC (Huang et al. 2021; Lu et al. 2021), highlighting its pivotal role in tumor progression. However, the intricate relationship between circPVT1 and the regulation of ferroptosis in NSCLC cells remains incompletely deciphered. In this study, we found that circPVT1 knockdown markedly enhanced oxidative stress, disrupted mitochondrial integrity, and modulated ferroptosis, underscoring its central role in the ferroptosis regulatory network within NSCLC. These results are not all unexpected, as circPVT1 plays a

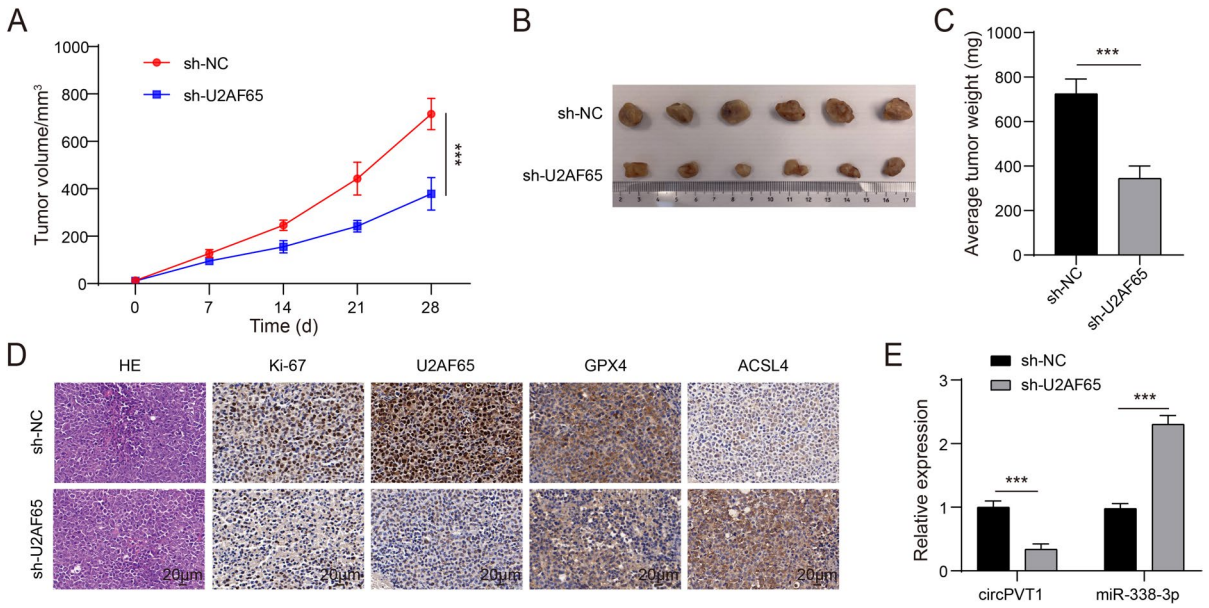

Fig. 8 U2AF65 promotes NSCLC tumorigenesis via the circPVT1/miR-338-3p/GPX4 axis. In xenograft models with U2AF65 knockdown: **A-C** Tumor volume and weight were measured. **D** H&E staining of tumor tissue and IHC staining detected the expression of Ki- 67, U2AF65, GPX4, and ACSL4. **E** qPCR was used to measure the expression of circPVT1 and miR-338-3p. $n = 6$, $^{***}P < 0.001$

pivotal role in cellular adaptation to oxidative stress and significantly contributes to cancer development (Zhong et al. 2019). However, the association between circPVT1 and mitochondrial function remains unclear, despite evidence that some circRNAs are closely related to mitochondrial dysfunction (Bravo et al. 2020). Furthermore, our research revealed that circPVT1 influences ACSL4, SLC7 A11, and PROM2 through GPX4 modulation, thereby inhibiting ferroptosis in NSCLC cells. Grube et al. have demonstrated that GPX4 silencing triggers ACSL4-associated ferroptosis (Grube et al. 2022). Additionally, previous study has found that circPVT1 silencing can promote ferroptosis by downregulating p-β-catenin, GPX4, and SLC7 A11 in esophageal cancer (Yao et al. 2021). Nonetheless, we are the first to report that circPVT1 modulates GPX4 expression, thereby suppressing ferroptosis in NSCLC cells.

Our mechanistic investigation delved into the sponge function of circPVT1, aiming to delineate its regulatory role in NSCLC ferroptosis. Utilizing the Starbase public database, miR-338-3p was predicted to potentially bind to circPVT1 as a regulatory miRNA. Subsequent assays validated their interaction and further revealed that silencing circPVT1 increased miR-338-3p levels, which was implicated in resistant NSCLC (Du et al. 2023), tumor metastasis (Lin et al. 2022), and progression (Zhu et al. 2021). Recent investigations start to explore its association with ferroptosis (Zhen et al. 2024; Zhou et al. 2022). Nevertheless, understanding of miR-338-3p role in ferroptosis, particularly in NSCLC, remains in its infancy.

Our focus was on determining the miR-338-3p targets related to ferroptosis, and identified GPX4 mRNA as a potential target. Further investigation confirmed their interaction and demonstrated miR-338-3p inhibitory effect on GPX4 expression. GPX4, initially identified by Ursini et al. through biochemical purification, is a crucial selenoprotein that catalyzes the reduction of phospholipid hydroperoxides in mammalian cells (Ursini et al. 1982). It is pivotal in ferroptosis regulation, acting as a critical anti-ferroptotic agent by enzymatically converting lipid hydroperoxides into non-toxic lipid alcohols, thus preventing lipid peroxidation within cellular membranes (Yang et al. 2014). This enzymatic activity is crucial for mitigating the accumulation of cytotoxic lipid-based ROS, positioning GPX4 as an essential suppressor of ferroptosis (Yang and Stockwell 2016). The deficiency or functional inhibition of GPX4 precipitates cellular vulnerability to ferroptosis, attributed to uncontrolled lipid peroxidation (Matsushita et al. 2015). Our results revealed that circPVT1 modulates ferroptosis in NSCLC via its sponge activity on miR-338-3p, thereby targeting and inhibiting GPX4 expression. This study expanded the understanding of the modulation mechanism of GPX4 and ferroptosis within its circRNA network.

In this study, U2AF65 was identified as the RBP of circPVT1 to stabilize it, and was found to enhance NSCLC cell proliferation and suppress ferroptosis by stabilizing circPVT1. Furthermore, U2AF65 can promote NSCLC tumorigenesis via the circPVT1/miR-338-3p/GPX4 axis. Research indicated that U2AF65 expression was elevated in NSCLC tissues, correlating with adverse prognosis and higher tumor stages (Blijlevens et al. 2021). Its overexpression was linked to the modulation of alternative splicing of pre-mRNA (Glasser et al. 2022), resulting in oncogenic isoforms that facilitated tumor progression (Laliotis et al. 2021). Nonetheless, its connection to ferroptosis and its specific mechanisms of action within NSCLC had yet to be fully elucidated. Our research bridged this gap by investigating the intricate relationship between U2AF65 and ferroptosis within the NSCLC context. By delineating how U2AF65, through stabilizing circPVT1 and influencing the circPVT1/miR-338-3p/GPX4 axis, contributes to ferroptosis regulation, this study uncovered novel mechanistic insights into NSCLC progression. Knowing how U2AF65 affects ferroptosis could provide new avenues for targeted therapeutic strategies, potentially leading to more effective treatments for NSCLC.

Author contributions Shenggang Liu is the guarantor of integrity of the entire study; Lujuan He and Jufen Wang contributed to the study concepts, study design and definition of intellectual content; Zezhi Zhou and Jiehan Jiang contributed to the literature research, experimental studies, data acquisition, data analysis and statistical analysis; Lujuan He, Zezhi Zhou and Shenggang Liu contributed to the manuscript preparation, manuscript editing and manuscript review.

Funding This work is supported by Hunan Natural Science Foundation (No. 2023JJ60073), Changsha Natural Science Foundation (No. kq2208436) and Hunan Natural Science Foundation (No. 2023JJ40071).

Data availability No datasets were generated or analysed during the current study.

Declarations

Ethical approval and consent to participate The patients involved in this study have written the informed consent. And the study was approved by the Ethics Committee of The Affiliated Changsha Central Hospital, Hengyang Medical School, University of South China (No. 2022-S0181).

The study was approved by the Ethics Committee of The Affiliated Changsha Central Hospital, Hengyang Medical School, University of South China (No. 2022-S0181).

Consent for publication Not applicable.

Competing interests The authors declare no competing interests.

References

Adhikary J, Chakraborty S, Dalal S, Basu S, Dey A, Ghosh A. Circular PVT1: an oncogenic non-coding RNA with emerging clinical importance. J Clin Pathol. 2019;72:513–9. https://doi.org/10.1136/jclinpath-2019-205891.

Arabpour J, Rezaei K, Khojini JY, Razi S, Hayati MJ, Gheibihayat SM. The potential role and mechanism of circRNAs in Ferroptosis: a comprehensive review. Pathol Res Pract. 2024;255:155203. https://doi.org/10.1016/j.prp.2024.155203.

Blijlevens M, Li J, van Beusechem VW. Biology of the mRNA splicing machinery and its dysregulation in cancer providing therapeutic opportunities. Int J Mol Sci. 2021;22. https://doi.org/10.3390/ijms22105110.

Bravo JI, Nozownik S, Danthi PS, Benayoun BA. Transposable elements, circular RNAs and mitochondrial transcription in age-related genomic regulation. Development. 2020;147. https://doi.org/10.1242/dev.175786.

Chen J, Zhao R, Wang Y, Xiao H, Lin W, Diao M, He S, Mei P, Liao Y. G protein-coupled estrogen receptor activates PI3K/AKT/mTOR signaling to suppress ferroptosis via SREBP1/SCD1-mediated lipogenesis. Mol Med. 2024;30:28. https://doi.org/10.1186/s10020-023-00763-x.

Dixon SJ, Lemberg KM, Lamprecht MR, Skouta R, Zaitsev EM, Gleason CE, Patel DN, Bauer AJ, Cantley AM, Yang WS, Morrison B 3rd, Stockwell BR. Ferroptosis: an iron-dependent form of nonapoptotic cell death. Cell. 2012;149:1060–72. https://doi.org/10.1016/j.cell.2012.03.042.

Dos Santos AF, Fazeli G, Xavier da Silva TN, FriedmannAngeli JP. Ferroptosis: mechanisms and implications for cancer development and therapy response. Trends Cell Biol. 2023;33:1062–76. https://doi.org/10.1016/j.tcb.2023.04.005.

Du L, Guo D, Sun C, Yan X, Lin S, Xu S. CircPIM3 regulates taxol resistance in non-small cell lung cancer via miR-338-3p/TNFAIP8 axis. Anticancer Drugs. 2023;34:115–25. https://doi.org/10.1097/CAD.0000000000001347.

Favorito V, Ricciotti I, De Giglio A, Fabbri L, Seminerio R, Di Federico A, Gariazzo E, Costabile S, Metro G. Non-small cell lung cancer: an update on emerging EGFR-targeted therapies. Expert Opin Emerg Drugs. 2024:1–16. https://doi.org/10.1080/14728214.2024.2331139.

Gao GB, Chen L, Pan JF, Lei T, Cai X, Hao Z, Wang Q, Shan G, Li J. LncRNA RGMB-AS1 inhibits HMOX1 ubiquitination and NAA10 activation to induce ferroptosis in non-small cell lung cancer. Cancer Lett. 2024;590:216826. https://doi.org/10.1016/j.canlet.2024.216826.

Glasser E, Maji D, Biancon G, Puthenpeedikakkal AMK, Cavender CE, Tebaldi T, Jenkins JL, Mathews DH, Halene S, Kielkopf CL. Pre-mRNA splicing factor U2AF2 recognizes distinct conformations of nucleotide variants at the center of the pre-mRNA splice site signal. Nucleic Acids Res. 2022;50:5299–312. https://doi.org/10.1093/nar/gkac287.

Grube J, Woitok MM, Mohs A, Erschfeld S, Lynen C, Trautwein C, Otto T. ACSL4-dependent ferroptosis does not represent a tumor-suppressive mechanism but ACSL4 rather promotes liver cancer progression. Cell Death Dis. 2022;13:704. https://doi.org/10.1038/s41419-022-05137-5.

Han S, Yang X, Zhuang J, Zhou Q, Wang J, Ru L, Niu F, Mao W. alpha-Hederin promotes ferroptosis and reverses cisplatin chemoresistance in non-small cell lung cancer. Aging (Albany NY). 2024;16:1298–317. https://doi.org/10.18632/aging.205408.

Hansen TB, Jensen TI, Clausen BH, Bramsen JB, Finsen B, Damgaard CK, Kjems J. Natural RNA circles function as efficient microRNA sponges. Nature. 2013;495:384–8. https://doi.org/10.1038/nature11993.

Huang M, Li T, Wang Q, Li C, Zhou H, Deng S, Lv Z, He Y, Hou B, Zhu G. Silencing circPVT1 enhances radiosensitivity in non-small cell lung cancer by sponging microRNA-1208. Cancer Biomark. 2021;31:263–79. https://doi.org/10.3233/CBM-203252.

Huang X, Wu S, Chen S, Qiu M, Zhao Y, Wei J, He J, Zhao W, Tan L, Su C, Zhou S. Prognostic impact of age in advanced non-small cell lung cancer patients

undergoing first-line checkpoint inhibitor immunotherapy and chemotherapy treatment. Int Immunopharmacol. 2024;132:111901. https://doi.org/10.1016/j.intimp.2024.111901.

Hummelink K, van der Noort V, Muller M, Schouten RD, Lalezari F, Peters D, Theelen W, Koelzer VH, Mertz KD, Zippelius A, van den Heuvel MM, Broeks A, Haanen J, Schumacher TN, Meijer GA, Smit EF, Monkhorst K, Thommen DS. PD-1T TILs as a Predictive biomarker for clinical benefit to PD-1 blockade in patients with advanced NSCLC. Clin Cancer Res. 2022;28:4893–906. https://doi.org/10.1158/1078-0432.CCR-22-0992.

Kamali MJ, Salehi M, Mostafavi M, Morovatshoar R, Akbari M, Latifi N, Barzegari O, Ghadimi F, Daraei A. Hijacking and rewiring of host CircRNA/miRNA/mRNA competitive endogenous RNA (ceRNA) regulatory networks by oncoviruses during development of viral cancers. Rev Med Virol. 2024;34:e2530. https://doi.org/10.1002/rmv.2530.

Khasraw M, Yalamanchili P, Santhanagopal A, Wu C, Salas M, Meng J, Karnoub M, Esker S, Felip E. Clinical management of patients with non-small cell lung cancer, brain metastases, and actionable genomic alterations: a systematic literature review. Adv Ther. 2024;41:1815–42. https://doi.org/10.1007/s12325-024-02799-9.

Laliotis GI, Chavdoula E, Paraskevopoulou MD, Kaba A, La Ferlita A, Singh S, Anastas V, Nair KA 2nd, Orlacchio A, Taraslia V, Vlachos I, Capece M, Hatzigeorgiou A, Palmieri D, Tsatsanis C, Alaimo S, Sehgal L, Carbone DP, Coppola V, Tsichlis PN. AKT3-mediated IWS1 phosphorylation promotes the proliferation of EGFR-mutant lung adenocarcinomas through cell cycle-regulated U2AF2 RNA splicing. Nat Commun. 2021;12:4624. https://doi.org/10.1038/s41467-021-24795-1.

Li J, Cheng D, Zhu M, Yu H, Pan Z, Liu L, Geng Q, Pan H, Yan M, Yao M. OTUB2 stabilizes U2AF2 to promote the Warburg effect and tumorigenesis via the AKT/mTOR signaling pathway in non-small cell lung cancer. Theranostics. 2019;9:179–95. https://doi.org/10.7150/thno.29545.

Li Z, Fan M, Zhou Z, Sang X. Circ_0082374 promotes the tumorigenesis and suppresses ferroptosis in non-small cell lung cancer by up-regulating GPX4 through sequestering miR-491-5p. Mol Biotechnol. 2024. https://doi.org/10.1007/s12033-024-01059-z.

Lin H, Gao Y, Sun K, Zhang Q, Li Y, Chen M, Jin F. COA3 overexpression promotes non-small cell lung cancer metastasis by reprogramming glucose metabolism. Am J Cancer Res. 2022;12:3662–78.

Livanou ME, Nikolaidou V, Skouras V, Fiste O, Kotteas E. Efficacy of NSCLC rechallenge with immune checkpoint inhibitors following disease progression or relapse. Cancers (Basel). 2024;16. https://doi.org/10.3390/cancers16061196.

Lu H, Xie X, Chen Q, Cai S, Liu S, Bao C, Luo J, Kong J. Clinical significance of circPVT1 in patients with non-small cell lung cancer who received cisplatin combined with gemcitabine chemotherapy. Tumori. 2021;107:204–8. https://doi.org/10.1177/0300891620941940.

Matsushita M, Freigang S, Schneider C, Conrad M, Bornkamm GW, Kopf M. T cell lipid peroxidation induces ferroptosis and prevents immunity to infection. J Exp Med. 2015;212:555–68. https://doi.org/10.1084/jem.20140857.

Ni J, Chen K, Zhang J, Zhang X. Inhibition of GPX4 or mTOR overcomes resistance to Lapatinib via promoting ferroptosis in NSCLC cells. Biochem Biophys Res Commun. 2021;567:154–60. https://doi.org/10.1016/j.bbrc.2021.06.051.

Okholm TLH, Sathe S, Park SS, Kamstrup AB, Rasmussen AM, Shankar A, Chua ZM, Fristrup N, Nielsen MM, Vang S, Dyrskjot L, Aigner S, Damgaard CK, Yeo GW, Pedersen JS. Transcriptome-wide profiles of circular RNA and RNA-binding protein interactions reveal effects on circular RNA biogenesis and cancer pathway expression. Genome Med. 2020;12:112. https://doi.org/10.1186/s13073-020-00812-8.

Padinharayil H, George A. Small extracellular vesicles: multifunctional aspects in non-small cell lung carcinoma. Crit Rev Oncol Hematol. 2024;198:104341. https://doi.org/10.1016/j.critrevonc.2024.104341.

Seibt TM, Proneth B, Conrad M. Role of GPX4 in ferroptosis and its pharmacological implication. Free Radic Biol Med. 2019;133:144–52. https://doi.org/10.1016/j.freeradbiomed.2018.09.014.

Tian W, Yang X, Yang H, Lv M, Sun X, Zhou B. Correction: exosomal miR-338-3p suppresses non-small-cell lung cancer cells metastasis by inhibiting CHL1 through the MAPK signaling pathway. Cell Death Dis. 2022;13:473. https://doi.org/10.1038/s41419-022-04933-3.

Ursini F, Maiorino M, Valente M, Ferri L, Gregolin C. Purification from pig liver of a protein which protects liposomes and biomembranes from peroxidative degradation and exhibits glutathione peroxidase activity on phosphatidylcholine hydroperoxides. Biochim Biophys Acta. 1982;710:197–211. https://doi.org/10.1016/0005-2760(82)90150-3.

Verduci L, Tarcitano E, Strano S, Yarden Y, Blandino G. CircRNAs: role in human diseases and potential use as biomarkers. Cell Death Dis. 2021;12:468. https://doi.org/10.1038/s41419-021-03743-3.

Wang Y, Zhang Y, Wang Y, Shu X, Lu C, Shao S, Liu X, Yang C, Luo J, Du Q. Using network pharmacology and molecular docking to explore the mechanism of Shan Ci Gu (Cremastra appendiculata) against non-small cell lung cancer. Front Chem. 2021;9:682862. https://doi.org/10.3389/fchem.2021.682862.

Wang L, Fu H, Song L, Wu Z, Yu J, Guo Q, Chen C, Yang X, Zhang J, Wang Q, Duan Y, Yang Y. Overcoming AZD9291 resistance and metastasis of NSCLC via ferroptosis and multitarget interference by nanocatalytic sensitizer plus AHP-DRI-12. Small. 2023;19:e2204133. https://doi.org/10.1002/smll.202204133.

Wang Z, Yao X, Wang K, Wang B. TFR1-mediated iron metabolism orchestrates tumor ferroptosis and immunity in non-small cell lung cancer. J Environ Pathol Toxicol Oncol. 2024;43:1–12. https://doi.org/10.1615/JEnvironPatholToxicolOncol.2023049084.

Xing N, Du Q, Guo S, Xiang G, Zhang Y, Meng X, Xiang L, Wang S. Ferroptosis in lung cancer: a novel pathway regulating cell death and a promising target for drug therapy.

Cell Death Discov. 2023;9:110. https://doi.org/10.1038/s41420-023-01407-z.

Yang WS, Stockwell BR. Ferroptosis: death by lipid peroxidation. Trends Cell Biol. 2016;26:165–76. https://doi.org/10.1016/j.tcb.2015.10.014.

Yang WS, SriRamaratnam R, Welsch ME, Shimada K, Skouta R, Viswanathan VS, Cheah JH, Clemons PA, Shamji AF, Clish CB, Brown LM, Girotti AW, Cornish VW, Schreiber SL, Stockwell BR. Regulation of ferroptotic cancer cell death by GPX4. Cell. 2014;156:317–31. https://doi.org/10.1016/j.cell.2013.12.010.

Yao W, Wang J, Meng F, Zhu Z, Jia X, Xu L, Zhang Q, Wei L. Circular RNA CircPVT1 inhibits 5-fluorouracil chemosensitivity by regulating ferroptosis through MiR-30a-5p/FZD3 axis in esophageal cancer cells. Front Oncol. 2021;11:780938. https://doi.org/10.3389/fonc.2021.780938.

Zhao R, Guan X, Zhang P, Liu Y, Xu Y, Sun C, Qiu S, Zhu W, Yang Z, Wang X. Development of postoperative bronchopleural fistula after neoadjuvant immunochemotherapy in non-small cell lung cancer: case reports and review of the literature. J Cancer Res Clin Oncol. 2024;150:175. https://doi.org/10.1007/s00432-024-05683-9.

Zhen S, Jia Y, Zhao Y, Wang J, Zheng B, Liu T, Duan Y, Lv W, Wang J, Xu F, Liu Y, Zhang Y, Liu L. NEAT1_1 confers gefitinib resistance in lung adenocarcinoma through promoting AKR1C1-mediated ferroptosis defence. Cell Death Discov. 2024;10:131. https://doi.org/10.1038/s41420-024-01892-w.

Zhong R, Chen Z, Mo T, Li Z, Zhang P. Potential Role of circPVT1 as a proliferative factor and treatment target in esophageal carcinoma. Cancer Cell Int. 2019;19:267. https://doi.org/10.1186/s12935-019-0985-9.

Zhou J, Zhang H, Zou D, Zhou Z, Wang W, Luo Y, Liu T. Clinicopathologic and prognostic roles of circular RNA plasmacytoma variant translocation 1 in various cancers. Expert Rev Mol Diagn. 2021;21:1095–104. https://doi.org/10.1080/14737159.2021.1964959.

Zhou J, Sun C, Dong X, Wang H. A novel miR-338-3p/SLC1A5 axis reprograms retinal pigment epithelium to increases its resistance to high glucose-induced cell ferroptosis. J Mol Histol. 2022;53:561–71. https://doi.org/10.1007/s10735-022-10070-0.

Zhu Y, Ma C, Lv A, Kou C. Circular RNA circ_0010235 sponges miR-338-3p to play oncogenic role in proliferation, migration and invasion of non-small-cell lung cancer cells through modulating KIF2A. Ann Med. 2021;53:693–706. https://doi.org/10.1080/07853890.2021.1925736.